inter.noise
HAMBURG 2016

Relating the statistical values of turbulence to the flow induced sound and resulting mechanical vibrations in multi-channel systems

Natalie Helena SCHLACHTER[1]; Manfred KALTENBACHER[2]

[1,2] Vienna University of Technology, Austria

ABSTRACT

Our multi-channel system consists of two parallel pipes which are joined in to a single, larger pipe and transmits a high speed flow of Reynolds number ranging between 0.7 and 1.8 million. The turbulence, which is amplified by combining the two flows, results in large fluctuations in the fluid pressure. These pressure fluctuations lead to the production of sound, which excites the acoustic resonances of the system and in turn causes mechanical vibrations in the pipe. Using hybrid numerical simulation techniques, the investigations show that the sound pressure level and mechanical displacement magnitudes are interdependent on the Reynolds number of the flow and the frequency of the acoustic resonance. This behavior is linked to the turbulent energy spectrum at the location of the largest sound source for a certain Reynolds number. The frequency content of the turbulent energy is shown to determine the amplitude of the acoustic resonances excited in the system, and thus the mechanical vibration magnitudes in the pipe.

Keywords: Duct, Turbulence, Vibroacoustics
I-INCE Classification of Subjects Number(s): 21.4, 21.6.6

1. INTRODUCTION

Various degrees of turbulence are always present in systems of ducts. This turbulence is increased by obstructions in the flow such as bends or junctions, or simply due to high flow speeds. A consequence of highly turbulent flow is large fluctuations in the pressure. The fluctuations consist of hydrodynamic and acoustic parts, and although the hydrodynamic fluctuations are magnitudes larger, it is the acoustic fluctuations that propagate through the system and instigate resonances. The additional vibrations in the system due to these acoustic pressures can be undesirable in industrial applications, for example due to increased fatigue, noise emission or interference with technical devices [1].

The investigated geometry is a multi-channel system typical for flow measurement devices, where one large inlet duct is split into two smaller, parallel ducts. After a certain distance, these ducts are once again joined in a larger outlet duct of the same diameter as the inlet, see figure 1. The two smaller, parallel ducts also contain three radial bends, such that an arch form is achieved.

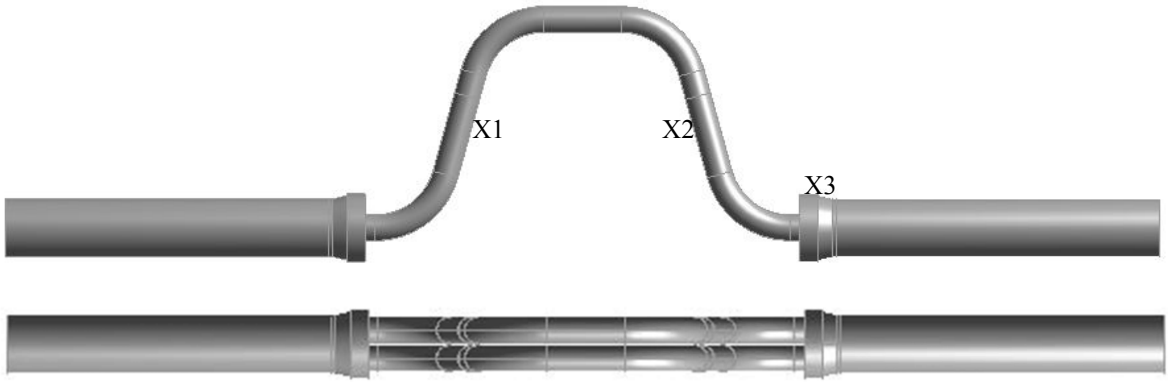

Figure 1 – A side and top view of the geometry used in the current analysis, with monitoring points X

[1] Natalie.Witkowski@tuwien.ac.at
2 Manfred.Kaltenbacher@tuwien.ac.at

The experimental investigation of the acoustic behavior near the source region is met with many difficulties due to the overlaying hydrodynamic pressures. For such cases, numerical simulation techniques prove invaluable and have also been applied in this work. The turbulence in the duct excites a broad spectrum of fluctuations since a turbulent flow by its nature is irregular and random. This means a deterministic approach to turbulence is impossible. Through numerical simulations, both the acoustics and statistical values of the turbulence may be evaluated, and it is the interdependence of the two in the channel flow over Reynolds number that shall be the focus of this paper.

2. ACOUSTIC ANALOGY

The two simulation methods with which the aeroacoustic quantities of a system may be deduced each have their own advantages and disadvantages. The first, more complicated method is to solve the full set of compressible Navier Stokes equations where both the fluid and acoustic quantities are resolved simultaneously. This method is both time and resource consuming, since it must be ensured that the small acoustic quantities, which can be up to several orders of magnitude smaller than the flow quantities, are accurately resolved [2]. Thus higher order methods are necessary and the specified boundary conditions must be nonreflecting. However, using this method, a bidirectional coupling of the acoustics and flow quantities can be achieved.

The second method is the hybrid approach. In this approach, the fluid dynamics of the system are resolved first. Thereafter, with the help of acoustic analogies, the acoustic source terms of the system may be deduced and the acoustic computation performed [2]. This method has its advantages in that when the flow is solved as incompressible, the acoustic quantities are obtained separately from the flow quantities und thus may be studied as a separate entity. This is useful when trying to understand the effects of the acoustics alone on the system in question. This approach only considers forward coupling, thus the influence of the sound on the flow field is assumed to be negligible [2].

For the present case, the hybrid method will be used. In order to resolve the acoustic quantities from the flow quantities the Lighthill acoustic analogy is applied [3]

$$\frac{1}{c_0^2}\frac{\partial^2 p'}{\partial t^2} - \Delta p' = \nabla \cdot \nabla \cdot T_{LH}, \tag{1}$$

where $c_0$is the speed of sound, p' the fluctuating pressure and T_{LH} the Lighthill tensor. This tensor describes the acoustic source in the flow field originating from unsteady convection, shear and other non-linear generation processes. For the incompressible flow case, the source term becomes [4]

$$\nabla \cdot \nabla \cdot T_{LH} = -\Delta p^{ic}, \tag{2}$$

with p^{ic} as the incompressible, or purely hydrodynamic, pressure. Additionally for the incompressible flow case, the perturbation equations [5, 6] may be applied,

$$p = \bar{p} + p' = \bar{p} + p^{ic} + p^a \tag{3}$$

which splits the overall pressure into the mean pressure $\bar{p}$, the fluctuating incompressible pressure p^{ic} and acoustic pressure p^a. When this splitting is applied to the conservation equations with $\nabla \cdot \bar{u} = 0$, the following relations result [6, 7]

$$\frac{\partial \boldsymbol{u}^a}{\partial t} + (\bar{\boldsymbol{u}} \cdot \nabla)\boldsymbol{u}^a + (\boldsymbol{u}^a \cdot \nabla)\bar{\boldsymbol{u}} + \frac{1}{\rho_0}\nabla p^a = 0 \tag{4}$$

$$\frac{1}{\rho_0 c_0^2}\left(\frac{\partial p^a}{\partial t} + \nabla \cdot (p^a \bar{\boldsymbol{u}})\right) + \nabla \cdot \boldsymbol{u}^a = \frac{1}{\rho_0 c_0^2}\frac{Dp^{ic}}{Dt} \tag{5}$$

where $\bar{\boldsymbol{u}}$ is the mean flow and $\boldsymbol{u}^a$ is the acoustic particle velocity. To simplify the above equations while still considering the mean flow [8], a scalar acoustic potential is introduced by $\boldsymbol{u}^a = -\nabla \emptyset^a$, which after combining the two equations results in the convected wave equation

$$\frac{1}{c_0^2}\frac{D^2\emptyset^a}{Dt^2} - \nabla\cdot\nabla\emptyset^a = -\frac{1}{\rho_0 c_0^2}\frac{Dp^{ic}}{Dt}. \quad (6)$$

Using this relation, the arising acoustic pressures can be calculated using only the incompressible fluid pressures and the mean velocity obtained in the fluid simulation, since $p^a = \rho_0 \frac{D\emptyset^a}{Dt}$. For a full derivation see [8].

3. NUMERICAL MODEL

3.1 Computational Fluid Dynamics Model

The fluid simulations were conducted on the Vienna Scientific Cluster using StarCCM+ double precision software. The fluid geometry was created as a single part with a velocity inlet, pressure outlet and the channel wall specified as boundaries.

The mesh was resolved containing between 1 million and 3 million polyhedral elements depending on the Reynolds number. The use of polyhedral elements greatly increased the convergence time of the simulations and required less mesh elements as, for example, a hexagonal mesh. Extrusions of the mesh were defined at the inlet and outlet boundaries. The extrusions were used to gradually increase the mesh element size over ten sequential element layers. This deemed useful in degrading the turbulent pressure structures leaving the system and helped in the prevention of reflections at the inlet and outlet boundaries. Any reflection of the flow or acoustic quantities in the CFD simulations can cause major discrepancies in the following acoustic simulations, and it must thus be ensured that the inlet and outlet are seen numerically as never-ending ducts.

A fully developed inlet profile was applied, which was obtained from a prior periodic flow simulation on the inlet diameter. Four flow rates were simulated, representing Reynolds numbers between 0.7 and 1.8 million. An initial steady simulation was conducted for 2500 steps to obtain the initial state of the system. From this state, the unsteady Detached Eddy Simulation was started. The time step was chosen either as 15µs and 10µs depending on the relevant Reynolds number and the required frequency band resolution. The turbulent system required an initial runtime of 0.3s until it had reached a stabilized state. Thereafter the simulation was run for a further and final 0.1s, where for every time step the incompressible pressure was written to a separate file for all fluid mesh elements. Additional pressure monitoring points were placed at certain locations of the pipe system, marked in figure 1, which are used in subsequent post-processing steps.

3.2 Vibroacoustics Model

The numerical acoustic model, comprising of both the fluid and the mechanical geometry, allows for a coarser mesh than the CFD model with only 100'000 to 300'000 tetrahedral elements. The pressure values written out in the preceding CFD simulations are used in the acoustic source term calculation as shown in equation (6), subsequently the acoustic source terms are interpolated to the acoustic mesh. The multiphysics software CFS++ [4] was used to solve the vibroacoustic problem.

Two boundary regions are defined at the inlet and outlet of the duct. These two regions act as perfectly matched layers for the absorption of the acoustic waves in all directions at the inlet and outlet [9]. This ensures that there are no unrealistic reflections back into the system. The time step and total simulation time is equal to that in the final fluid simulation. The output of the simulation is the acoustic pressure over the fluid volume, which may be viewed in the time or frequency domain. With the chosen time steps, simulation time and mesh size a well-defined frequency spectrum between 10 Hz and 2000 Hz, with a resolution of 10 Hz, is obtained. Since the frequency range to be studied lies under 1000 Hz, this spectrum range should be sufficient. The resolution of 10 Hz sometimes resulted in under-defined resonance modes, but the main resonances could still be observed. In future simulations, at the cost of increased simulation time, this resolution could be improved.

The fluid region is directly coupled to the mechanical region in the model, such that the mechanical displacements caused by the acoustic pressure acting on the wall surfaces may be analyzed. The acoustic pressures and mechanical displacements were written out for all fluid and mechanical nodes respectively at each time step. As in the CFD analysis, monitoring points were defined near the area of largest turbulence at the outlet, and along the two smaller parallel pipes, where the mechanical excitation is of particular interest.

4. FLOW AND VIBROACOUSTIC SIMULATION RESULTS

Using the Q-criterion to visualize the vortices in the flow simulation results, the main turbulence areas can be identified. Disturbances to the flow can be seen at the radius bends, and also slightly at the inlet channel where the flow is separated. Large turbulence occurs at the outlet of the duct where the two smaller flows are joined. Figure 2 shows a comparison of the turbulence at the inlet and outlet areas for a certain Reynolds number. Since the outlet region shows the greatest velocity fluctuations, it is also expected to be the main acoustic source.

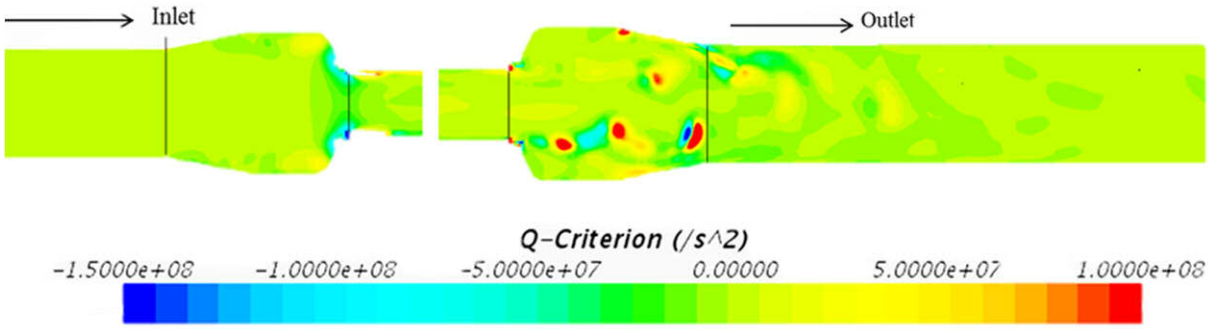

Figure 2 – Q-Criterion visualization in a sample CFD simulation at the end time for the inlet (left) and outlet (right) areas

This prediction is confirmed by the acoustic simulation results. At all simulated Reynolds numbers the location of the main acoustic source was found to lie at the channel outlet where the two flows are joined. In figure 3 a contour plot is shown, locating the maximum acoustic source amplitudes as described in equation (6) at a certain frequency.

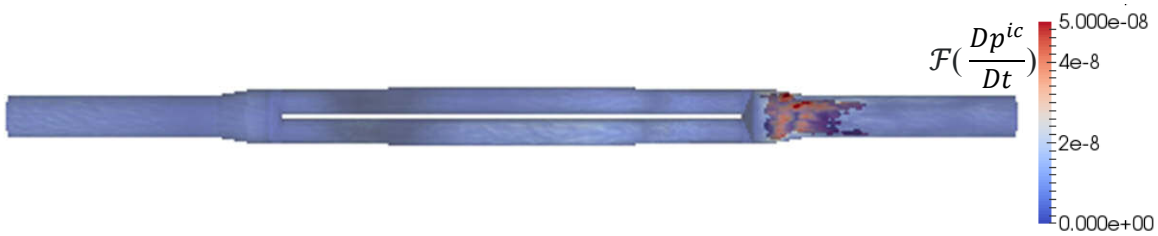

Figure 3 – Main acoustic sources are located at the outlet channel for all flow rates

The acoustic source at the outlet is larger than those at the radius bends and inlet over the entire frequency spectrum. The effect of this acoustic sound source on the system can best be seen in the results of the vibroacoustic analysis, namely the acoustic pressures and mechanical displacements, when viewed in the frequency domain. The plot in figure 4 shows the power spectral density of the sound pressure level at monitoring point X1 (figure 1) for all Reynolds numbers. Large peaks in the amplitude occur at specific frequencies, for example at 195 Hz, 390 Hz and 585 Hz.

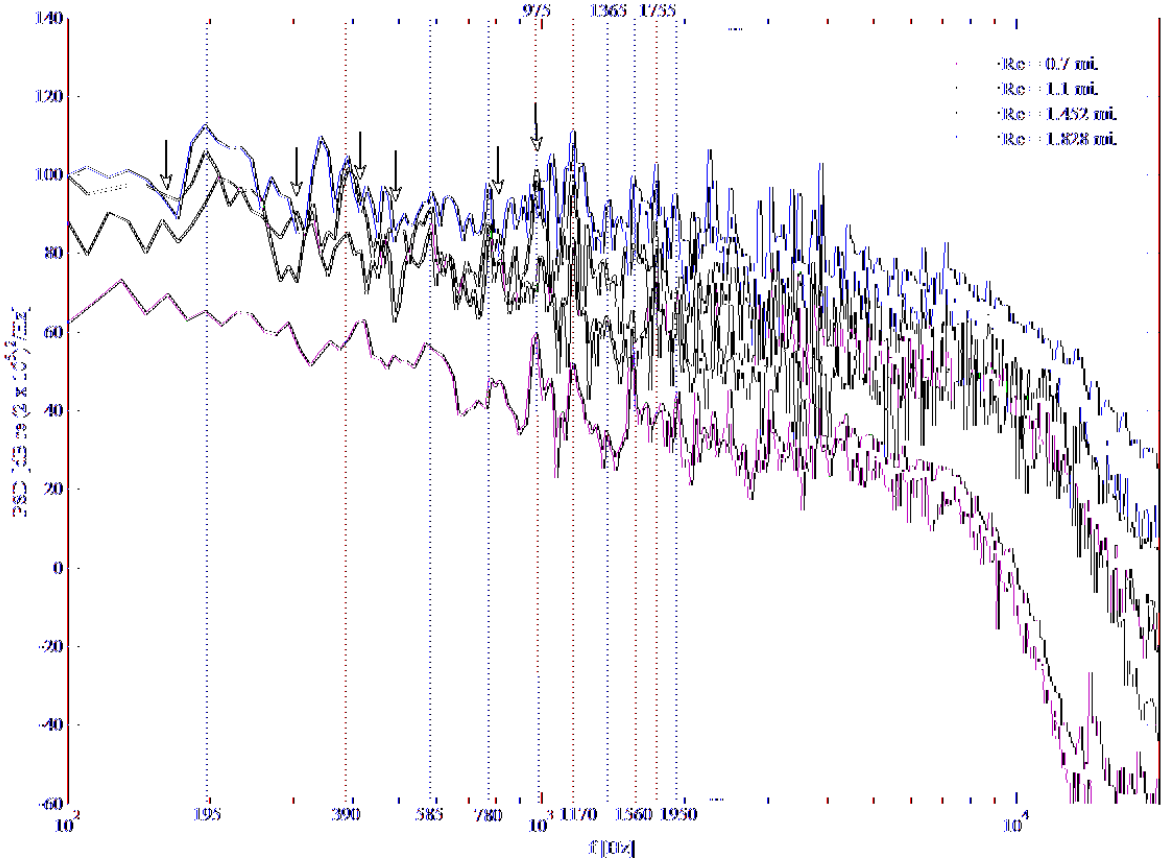

Figure 4 – Power spectral density of sound pressure at monitoring point X1 over Reynolds number

These peaks are present at the same frequencies for all calculated Reynolds numbers, and correspond to the acoustic resonances excited between the two points where the flow is separated and joined. All acoustic resonances present due to the geometry form are excited by the broadband sound source at the outlet, but the largest occur within the smaller channels and are marked by dotted lines in figure 4. Such an acoustic resonance can be visualized by looking at the acoustic pressures over the whole fluid volume in the frequency domain, for example the first and second acoustic resonances in the fluid pictured at the top of figure 5. The acoustic resonances result in the mechanical displacement of the channel geometry since the acoustic pressures interact with the duct walls. The mechanical displacements are greatest where the acoustic pressures are of largest amplitude, as pictured in the bottom of figure 5.

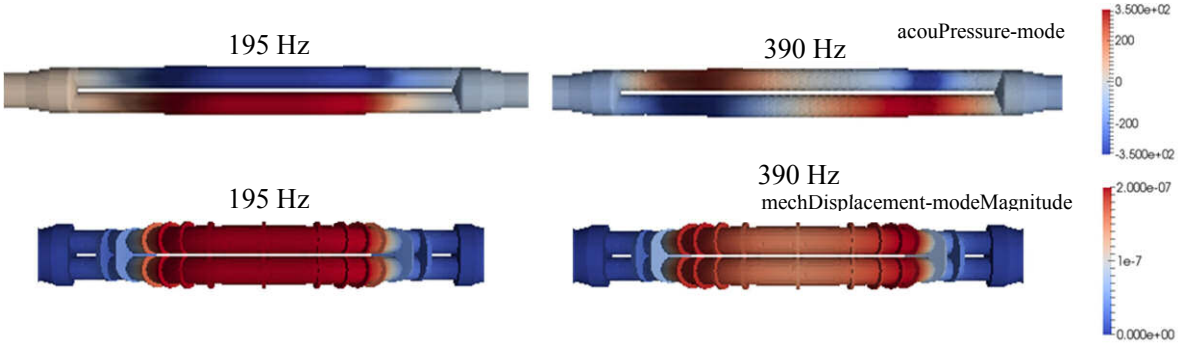

Figure 5 – The first and second acoustic resonances in the fluid (top) and the corresponding mechanical displacements (bottom)

If we look at the power spectral density of the mechanical displacement at monitoring point X1 over the frequency as in figure 6, it can be observed that the peaks in the displacement amplitudes occur at the same frequencies as the acoustic resonances occur in the fluid, and are also marked with dotted lines as in figure 4.

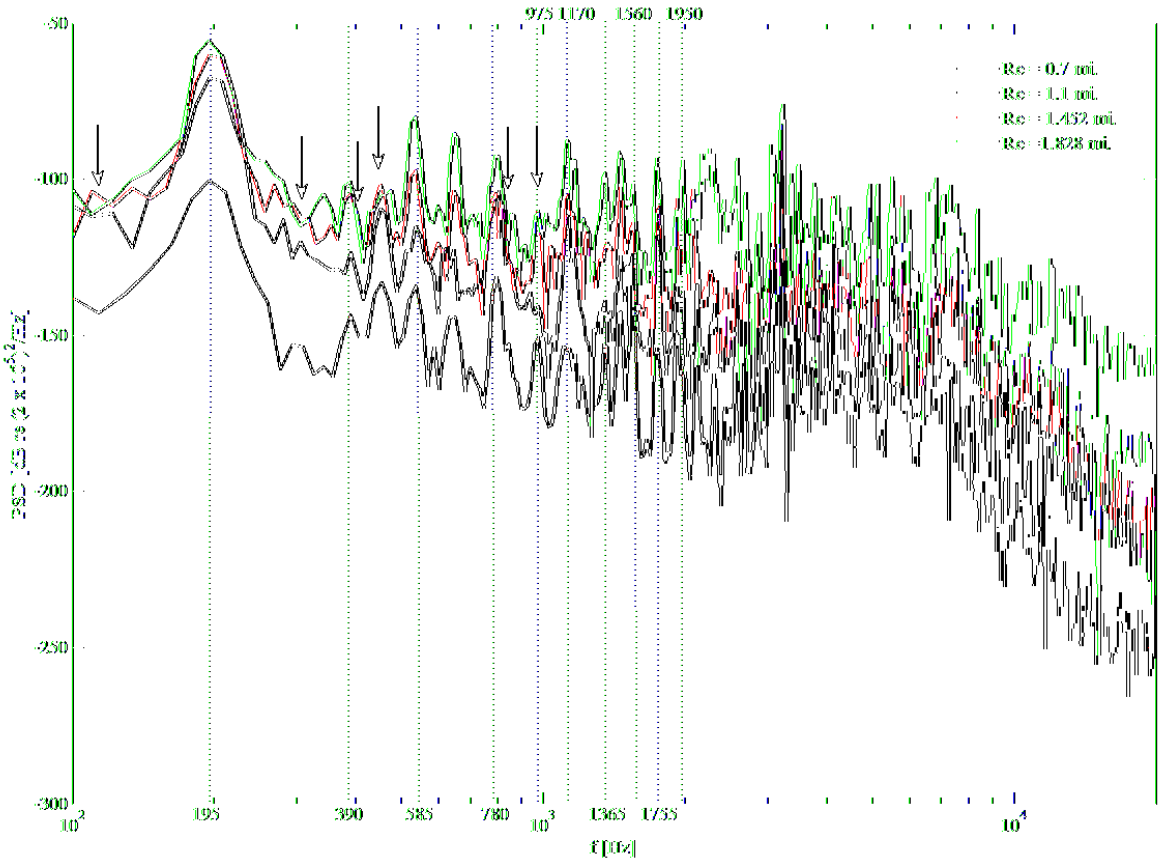

Figure 6 – Power spectral density of geometrical displacement (perpendicular to flow) at monitoring point X1 in frequency domain

An intriguing, and perhaps at first confusing, result is that the largest amplitudes of the sound pressure level or mechanical displacement at certain frequencies does not always correspond to the highest Reynolds number. In figures 4 and 6, amplitude peaks have been marked with colored arrows to indicate frequencies at which the sound pressure level and mechanical displacement is larger for as smaller Reynolds number. In this case, only the two highest Reynolds number plots relating to 1.4 and 1.8 million are compared. The amplitude peaks in these graphs are higher for a Reynolds number of 1.4 million at frequencies around 160Hz, 300Hz, 420Hz, 490Hz, 820Hz and 980Hz.

This indicates that the outlet turbulence contains a specific acoustic pressure frequency spectrum depending on the Reynolds number, and it is reproducible. In this regard, it is interesting to study the statistical values of the turbulence at the outlet area for different Reynolds numbers.

5. STASTICAL VALUES OF TURBULENCE

A turbulent flow is by its nature irregular and random, which means a deterministic approach to turbulence is impossible [10]. Turbulence excites a broad spectrum of fluctuations observant in most turbulent quantities such as the velocity [11]. The turbulence energy spectrum is a method used to display the energy content of the turbulence over wavenumber or frequency. It is defined using a correlation tensor R_{ii} between velocities at two different points separated by a distance r [10],

$$R_{ii}(r,t) = \langle u_i(x,t)u_i(x+r,t)\rangle \tag{7}$$

where u_i is the velocity component with defined spatial direction i. Since the turbulent velocity field is assumed to be homogeneous and isotropic the correlation tensor is a function only of the distance between the two points and not on their location. The three dimensional energy spectrum is then

$$E(f) = \frac{1}{2}\mathcal{F}[R_{11}(r,t) + R_{22}(r,t) + R_{33}(r,t)] \tag{8}$$

which, by performing the Fourier transform yields

$$E(f) = \frac{1}{2}\sum_{i=1,3} \tilde{u}_i(f)\tilde{u}_i^*(f) \tag{9}$$

where $\tilde{u}_i(f)$ is the Fourier transform of the velocity in the ith direction and its conjugate is marked with *. When applying this correlation to the outlet area, the location of the selected points must be considered carefully, with as many points used as efficiently possible. In this geometrical case, when points were chosen too far downstream from the outlet, an incorrect representation of the energy spectrum was obtained, since as it is now known, the most important acoustic source occurs quite directly at the joining of the two flows. It is then directly in this area in which the points for such an analysis should be chosen. The energy spectrum for the four Reynolds numbers at the outlet area of the geometry is shown in figure 7.

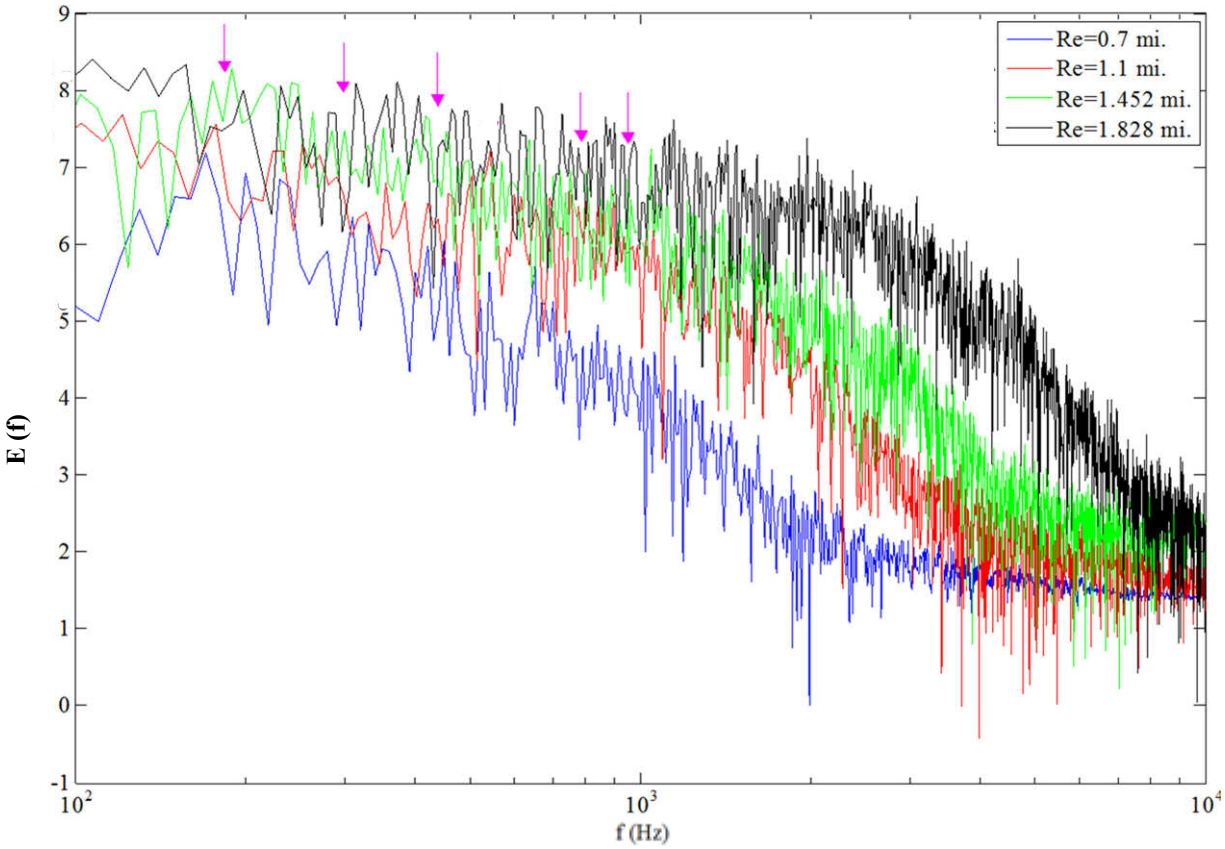

Figure 7 – Energy spectrum taken from points at the outlet of the geometry at four Reynolds numbers

It is observed that at specific frequencies the magnitude of the energy spectrum is larger at a Reynolds number of 1.4 million than 1.8 million, as in the simulation results. The position of these frequencies is marked again using colored arrows and corresponds to the same frequencies observed in figures 4 and 6, namely around 160Hz, 300Hz, 420Hz, 490Hz, 820Hz and 980Hz. A similar figure, as in figure 8, is achieved by plotting the power spectral density of the acoustic pressures at monitoring point X3. Once again, the amplitude differences are present at the same frequencies as in the previous figures.

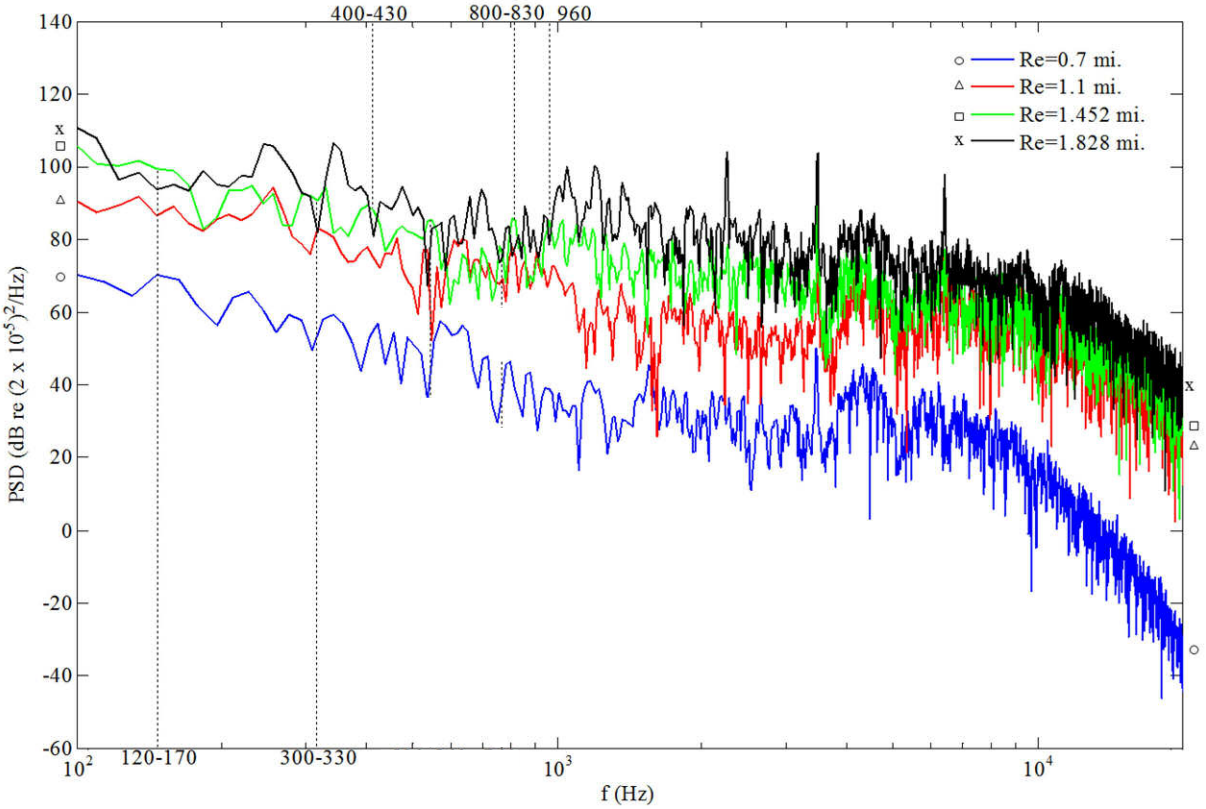

Figure 8 – Power spectral density of the sound pressure level at monitoring point X3

The turbulence energy spectrum over the Reynolds number confirms that the behavior of the acoustic pressure in the smaller pipes is controlled by the behavior of the main acoustic source at the outlet over Reynolds number. At the same frequencies that can be identified in figures 4 and 6, the energy content of the turbulence is greater. This causes an increase in the acoustic pressure and mechanical displacements at the monitoring points in the smaller pipes. This means the energy content of the turbulence at these frequencies is Reynolds number dependent and reproducible.

6. VERIFICATION OF RESULTS

It is important to verify if this interdependency of the turbulence frequency spectrum and the acoustic pressure amplitudes is purely numerical or if it can also be observed in experiments. The geometry as described was constructed and built into a gas flow rig. Two laser vibrometers are used to capture the displacements on two points of the inner channels, matching the locations of two of the monitoring points X1 and X2 in the simulation models. The laser vibrometers could only capture the velocity magnitude at the monitoring points. Air under 10 bar was allowed to flow through the rig for the four Reynolds number cases. The displacements at the two points were captured with help of an oscilloscope, saving the velocity magnitude values at the monitoring points over a time period. An increased level of noise is present in the gas rig due to the presence of other components such as the pump and valves. Additional acoustic resonances also occur due to the rig geometry which consists of many bends and junctions, in comparison to the simulation which simply assumed never ending channels. It is thus difficult to compare the simulation and measurement results directly. Nevertheless, the acoustic resonances present in the simulations could be identified in the measurement results. More importantly, peaks in the vibration magnitudes are seen to be higher at the specific frequencies for a Reynolds number of 1.4 million compared to 1.8 million, see Figure 9 for a comparison of the results for these two Reynolds numbers. As in figures 4 and 6, the frequencies showing higher amplitude peaks at a lower Reynolds number are marked with arrows in figure 9. The same peaks are once again present around 160Hz, 420Hz, 490Hz and 820Hz. Since the pipes were oscillating at 280Hz during this measurement, as typical for measurement devices of this type, the peak at 300Hz is overlapped but may be derived from the larger peaks occurring before it at around 250Hz. This verifies that the turbulent energy spectrum was correctly modeled, and the statistical values of this turbulence are reproducible for different Reynolds numbers.

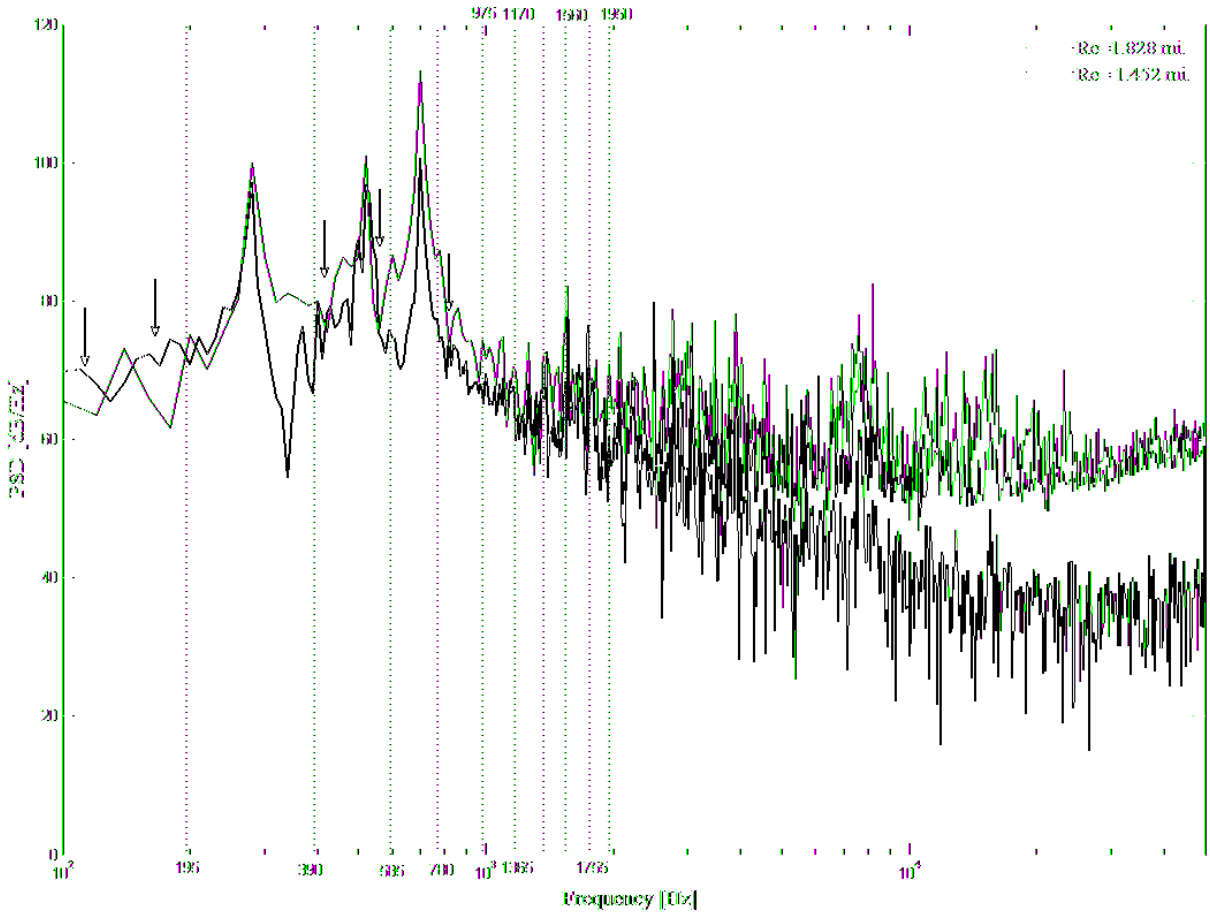

Figure 9 – Power spectral density of the velocity magnitude at monitoring point X1

7. CONCLUSIONS

The flow induced sound in a multi-channel geometry at different Reynolds numbers has been investigated. The hybrid method of computational aeroacoustics has been applied, allowing the separation of the acoustic and hydrodynamic values in the near field region. The main acoustic source, of a broadband nature, was found to be located at the outlet duct after the rejoining of the two parallel flows for all Reynolds numbers. As a result, peaks in the amplitude of the acoustic pressure and mechanical displacement frequency spectrums could be identified, which correlate to the acoustic resonances within the system, mainly between the flow separation and joining regions. A phenomenon was observed, where for certain lower Reynolds numbers, larger amplitudes of the peaks occurred than for higher Reynolds numbers, giving the system a non-linear behavior. This can be explained once a turbulence energy spectrum has been computed for the source location. The acoustic source contains a different frequency distribution depending on the Reynolds number, and thus an acoustic resonance may be more excited at one Reynolds number than the other - even if this Reynolds number is lower. These numerical results could be verified with experiments conducted on a gas flow rig.

ACKNOWLEDGEMENTS

The computational results presented here have been achieved in part using the Vienna Scientific Cluster (VSC). The CFD simulations have been made possible with the provision of a StarCCM+ academic license.

REFERENCES

1. Ziada S. Flow-excited acoustic resonance in industry. Journal of Pressure Vessel Technology 132 (2010); 19.
2. Wagner C, Hüttl T, Sagaut P (eds.). Large-Eddy Simulation for Acoustics. Cambridge University Press; 2007.

3. Lighthill MJ. On Sound Generated Aerodynamically. I. General Theory. Proceedings of the Royal Society of London; 1952.
4. Kaltenbacher M. Numerical Simulation of Mechatronic Sensors and Actuators - Finite Elements for Computational Multiphysics. Springer 3rd ed.; 2015.
5. Ewert R, Schroeder W. Acoustic Perturbation Equations based on Flow decomposition via Source Filtering. Journal of Computational Physics 188 (2003); 365398.
6. Hüppe A, Kaltenbacher M. Spectral Finite elements for computational aeroacoustics using acoustic perturbation equations. Journal of Computational Acoustics 20 (2012).
7. Hüppe A. Spectral Finite Elements for Acoustic Field Computation. Ph.D. Thesis; Alpen-Adria-Universität Klagenfurt; Austria 2013.
8. Hüppe A, Grabinger J, Kaltenbacher M, Reppenhagen A, Dutzler G, Kuehnel W. A Non-conforming Finite Element Method for Computational Aeroacoustics in Rotating Systems. 20th AIAA/CEAS Aeroacoustics Conference; 2014.
9. Kaltenbacher B, Kaltenbacher M. I.Sim: A modified and stable version of a perfectly matched layer technique for the 3-d second order wave equation in time domain with an application to aeroacoustics. Journal of Computational Physics; 2013.
10. Haugen N.E.L. Energy Spectra and scaling relations in numerical turbulence with laboratory and astrophysical applications. Ph.D. Thesis; Norwegian University of Science and Technology; 2004.
11. Wilczek M, Narita Y. Wave number frequency spectrum for turbulence from a random sweeping hypothesis with mean flow. American Physical Society; Physical Review E 86; 066308 2012.